The Role of Nanoparticle Layer Separation in the Finite Deformation Response of Layered Polyurethane-Clay Nanocomposites

Amit K. Kaushik,[†] Paul Podsiadlo,[‡,#] Ming Qin,[‡] Charles M. Shaw,[¶] Anthony M. Waas,[§,†] Nicholas A. Kotov,[‡,||,⊥] and Ellen M. Arruda*,[†,¶]

[†]*Department of Mechanical Engineering and* [‡]*Department of Chemical Engineering,* [§]*Department of Aerospace Engineering and* [||]*Department of Biomedical Engineering and* [⊥]*Department of Material Science and Engineering, University of Michigan, Ann Arbor, Michigan 48109.* [#] *Current address: Argonne National Laboratory, Center for Nanoscale Materials, 9700 Cass Ave., Bldg. 440, A132C, Argonne, IL 60439.* [¶] *Program in Macromolecular Science and Engineering, University of Michigan*

ABSTRACT: Nanoscale control of structure in polymer nanocomposites is critical for their performance but has been difficult to investigate systematically due to the lack of a suitable experimental model. In this work, we investigated the role of nanoparticle layer separation in the finite deformation response of layered polyurethane− (PU−) montmorillonite (MTM) nanocomposites. A series of multilayered nanocomposites was manufactured, with alternating PU and MTM nanolayers, using a layer-by-layer manufacturing technique. The systematic variation in MTM nanoparticle volume fraction was achieved by varying the thickness of the PU nanolayer and therefore the MTM layer separation. Traditional polymer nanocomposite blending techniques result in a wide variation in nanoparticle separation for a given nanocomposite. In this investigation, we controlled the MTM nanoparticle layer separation, which allowed us to examine its effect on the nanocomposite response over a broad range in nanoparticle volume fraction. The PU−MTM nanocomposites demonstrated an increasing yield strength and stiffness with increased MTM volume fraction or reduced nanoparticle layer separation. A transition from ductile to brittle behavior in the stress−strain constitutive response was observed at a high volume fraction of MTM nanoparticles. We demonstrate that a critical nanoparticle separation exists, below which brittle behavior dominates the response of PU−MTM nanocomposites.

Introduction

Over the last 2 decades, the manufacture of nanocomposites has received much attention both by academics and by industry.[1−5] For polymer nanocomposites, strides have been made to incorporate large volume fractions of nanofillers into various polymer matrices, thereby enhancing their physical, thermal and mechanical properties.[2−4,6−12] Examples of nanofillers used include carbon nanotubes (CNTs), clay nanoparticles, and cellulose nanocrystals. These nanofillers have at least one characteristic dimension of the order of nanometers and can range from isotropic elements to highly anisotropic materials. Their geometries can vary from disks to needle-like shapes. While CNTs are cylindrical in shape and cellulose nanocrystals are rod-like elements, clay nanoparticles have a disk-like shape. The advantage of using nanofillers over traditional fillers is that these nanomaterials garner most of their enhancements from interactions on the molecular scale influencing the physical and mechanical properties at a scale inaccessible by traditional microcomposites.

The efficacy of reinforcement depends on the nanofiller aspect ratio, its mechanical properties and the interaction between the matrix and the nanofiller. Clay nanoparticles have been proposed to be an ideal reinforcement for tuning the bulk properties of polymer matrices because of their extremely high aspect ratio. The high-aspect ratio results in an increased surface-to-volume ratio that enhances the effective load transfer between the matrix and the clay nanoparticles. Moreover, clay nanoparticles display high in-plane strength and stiffness.[13,14]

Polymer−clay nanocomposites represent a relatively new class of hybrid materials that has received widespread interest in the research community.[2−8,11−13,15−26] This interest is fueled by the promise of unprecedented performance, design flexibility, and optimization. Despite consistent efforts by research groups worldwide, however, persistent challenges with poor miscibility and dispersion of nanoparticles, especially at high volume fractions, have prevented nanocomposites from realizing their full potential.[12,19,24] Notwithstanding a decent increase in properties at low volume fractions of clay nanoparticles, most reported nanocomposites exhibit marginally increased or even decreased mechanical properties at high volume fractions.[4,16,18] This is most likely due to a lack of control over the nanoparticle separation, which results in an aggregation of nanoparticles or, at best, a local variation in nanoparticle spacing leading to local regions that are structurally weak or brittle. For this reason, it is very difficult to investigate these nanocomposites systematically to understand and optimize their performance. Nanoscale structural parameters such as the separation between MTM nanoparticles have tremendous effects on the mechanical properties of the nanocomposites, yet have proven difficult to vary consistently and uniformly. This limits the efficient design and understanding of the effect of clay nanoparticles in the polymer matrix. The ability to disperse a wide range of volume fractions of nanoparticles within polymers while retaining consistent structural organization is crucial to optimally design nanocomposites for their various applications.

*Corresponding author. E-mail: arruda@umich.edu.

The goal of the present study is to investigate the role of nanoparticle separation in the finite deformation of PU−MTM nanocomposites. We further discuss the stiffening and toughening mechanisms at the nanoscale by which MTM nanoparticles provide enhancement in mechanical properties. Moreover, we demonstrate our capability to access a wide range of volume fractions of the clay nanoparticles in the PU matrix, without compromising on the dispersion of nanoparticles. This enables design optimization in terms of stiffness, strength and toughness of these nanocomposites. To the best of our knowledge, our findings represent the first example of a nanocomposite system in which a wide range of volume fractions of clay nanoparticles has been accessed with a controlled nanoparticle separation allowing us to examine its effect on nanocomposite response.

We approach the preparation of these nanocomposites using the well-known layer-by-layer (LBL) manufacturing technique.[27,28] LBL manufacturing is the sequential deposition of oppositely charged nanolayers that may include polyelectrolytes, nanoparticles, nanowires, clay nanoplatelets, proteins, DNA, dyes, and other materials. LBL provides the capacity to combine macromolecules with nanometer scale homogeneity that are otherwise difficult or impossible to combine. The striking characteristic of LBL that separates it from the conventional manufacturing methods is the unprecedented control it provides over the structure at the nanoscale. The multilayered structures prepared using the LBL technique offer the potential to conduct well-controlled experiments to examine the property enhancement mechanisms in nanocomposites at the nanoscale.

Experimental Details

Materials. A semitransparent cationic polyurethane (PU) dispersion with a specific gravity of 1.02 g/cm^3 (at 25 °C) was obtained from HEPCE CHEM Co. Ltd. (Kyungki-Do, Korea). The PU was prepared from isophorene diisocyanate (IPDI), poly(tetra[ethylene glycol]) (PTMG) and 3-diethylamino-1, 2-propanediol (DEAPD). Ethylene diamine was added as a chain extender. The concentration and molecular weight of as-received PU was 35 wt % and 90 000 respectively. Various concentrations of PU were prepared by adding the required amount of deionized water and stirring before use.

Na^+−montmorillonite (MTM) (Cloisite Na^+) clay with a specific gravity of 1.98 g/cm^3 was purchased from Southern Clay Products (Gonzales, TX). The as-received MTM nanoparticles were disk-like elements of thin silicate layers, 1 nm thick and ranging in diameter from 100 to 1000 nm, the average diameter being 110 nm as described by the manufacturer. A 0.5 wt % dispersion of MTM nanoparticles was used for the preparation of nanocomposites. Then 5 g of the as-received MTM clay was dissolved in 1 L of 18 $MΩ cm^{-1}$, pH = 5.6 deionized water under vigorous stirring for 1 week. This resulted in the exfoliation of clay into silicate layers due to the solvation of Na^+ cations holding them together.[29] After one week, the nondispersible fraction was allowed to precipitate and the supernatant was collected.

Nanocomposites were prepared on 25 mm × 75 mm microscope glass slides obtained from Fisher Scientific (Waltham, MA). Hydrogen peroxide and concentrated sulfuric acid used for cleaning the glass slides were purchased from Sigma-Aldrich (St. Louis, MO). A 1 vol % sample of concentrated hydrofluoric acid (Sigma-Aldrich), prepared by appropriate dilution with deionized water, was used for detaching the nanocomposite films from the glass slides. 2-Propanol, ACS grade, used for the treatment of free-standing nanocomposite films, was also purchased from Sigma-Aldrich.

Synthesis. Pure PU films were cast from the as-received dispersion by diluting with deionized water and drying overnight in an oven at a temperature of ∼80 °C.

The PU−MTM nanocomposites were prepared using the layer-by-layer (LBL) manufacturing technique.[27,28,30,31] A microscopic glass slide was first immersed into a solution of PU leading to deposition of a nanolayer of the PU on the glass slide (step 1). The slide was then rinsed with deionized water to remove the excess material (step 2). The rinsing step was followed by immersion in the MTM nanoparticles dispersion (step 3), resulting in deposition of a nanolayer of MTM nanoparticles on the PU nanolayer. This step was again followed by rinsing with deionized water (step 4). The rinsing steps were followed by drying with compressed air to remove excess water. Each deposition cycle, consisting of steps 1−4, resulted in the deposition of a nanocomposite bilayer. Due to the molecular nature of the layers deposited in each cycle, the LBL manufacturing technique affords nanometer scale precision in the thin film thickness. The deposition cycle can be repeated as many times as required to build a multilayered nanocomposite of desired thickness. In the PU−MTM nanocomposites preparation, the deposition cycle was repeated 300 times to produce 300-bilayer nanocomposites. The immersion time in the PU and MTM nanoparticles dispersion was 5 min; the rinsing and drying times were 2 and 1 min, respectively. The preparation of the nanocomposites was accomplished using a Strato-Sequence IV, a robotic dipping machine, from Nanostrata Inc. (Tallahassee, FL).

The 300-bilayer nanocomposites were separated from the microscopic glass slide using HF.[32] The free-standing nanocomposite films were then treated overnight with isopropanol and finally dried in an oven at a temperature of ∼80 °C.

The loading of MTM nanoparticles was varied in the PU−MTM nanocomposites by varying the dilution of the PU in the LBL manufacturing process. The PU was diluted, using deionized water, from 3 to 75 times the as-received concentration to manufacture nanocomposites with various loadings of MTM nanoparticles.

Characterization. The loading of MTM nanoparticles in the nanocomposites was determined using a Thermogravimetric Analyzer (TGA) Pyris 1 from Perkin-Elmer (Waltham, MA). A sample with a weight ranging from 0.1 to 0.5 mg was heated at a temperature ramp-up rate of 10 °C/min while being purged with air at a flow rate of 20 mL/min. The MTM loading was determined by measuring the loss in weight of the sample with temperature as compared to the pure polymer. The polymer burnt off completely and the remaining weight was used to determine the weight fraction of MTM nanoparticles. The measured weight fraction was converted to the volume fraction by the following formula:

$$v_c = \frac{w_c \rho_p}{\rho_c(1 - w_c) + w_c \rho_p} \tag{1}$$

where v_c is the volume fraction of MTM nanoparticles, w_c is the weight fraction of MTM nanoparticles obtained from TGA and ρ_c and ρ_p are the densities of MTM clay and PU respectively. The data are represented as mean ± SD, each of them determined from three different samples.

A Rigaku Rotaflex Cu Kα rotating anode diffractometer (λ = 1.54) was used to perform the X-ray diffraction measurements. Samples were tested on the surface perpendicular to the thickness direction in a $\theta - 2\theta$ geometry and were scanned from a 2θ of 3−35° at a scanning rate of 3°/min with a sampling interval of 0.05.

The thickness of the PU−MTM nanocomposites was determined using a FEI Nova Nanolab dual-beam focused ion beam and scanning electron microscope (SEM). Because of the nonconductive nature of the PU−MTM nanocomposites, a few nanometers thick layer of gold was sputtered onto their cross sections prior to imaging. The thicknesses are represented as mean ± SD, each of them determined from at least three different samples. The average bilayer thickness was determined
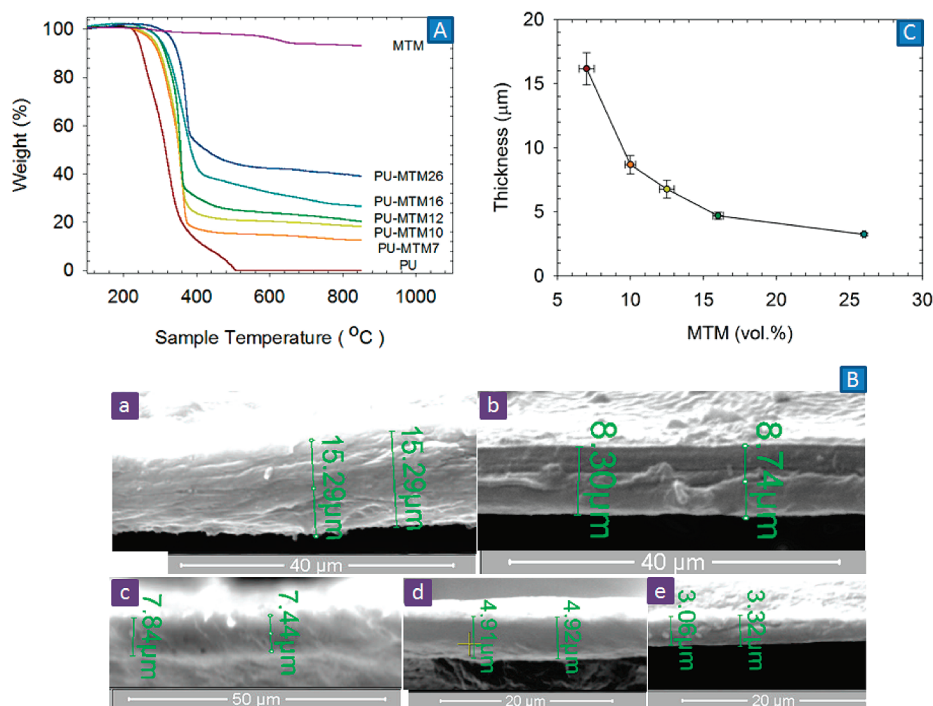
Figure 1. (A) Thermogravimetric Analysis for PU, a series of PU−MTM nanocomposites and MTM clay. (B) Typical SEM images showing cross sections of (a) 7 vol %, (b) 10 vol %, (c) 12 vol %, (d) 16 vol %, and (e) 26 vol % 300-bilayer PU−MTM nanocomposite. (C) Thickness of 300-bilayer PU−MTM nanocomposites as a function of volume fractions of MTM nanoparticles. Error bars indicate the uncertainty in thicknesses and volume fractions.

by dividing the mean value of nanocomposite thickness by its number of bilayers.

Mechanical characterization was performed using an in-house designed tensile tester.[33] The dog bone specimens were loaded at a constant strain rate of 0.005/s at room temperature (∼23 °C) and humidity of ∼30% until failure and the synchronized force and image recordings were compiled using LAB-VIEW. Analysis of actual material strain was achieved by adhering 25 μm diameter microspheres on the specimen surface. The specimen images were analyzed with Metamorph software from Meta Imaging to track the microsphere positions. At least three dog-bone specimens with a gauge length of ∼7 mm and width of ∼1 mm were tested in order to produce each representative stress−strain curve. The raw force vs image data were converted to nominal stress (force/cross-section area) vs nominal strain data (change in separation of microspheres/ initial separation). Modulus was determined by calculating the initial slope of the nominal stress vs nominal strain data. The gage section of the dog bone specimens deformed homogeneously with no predominant necking phenomena. The true stress−strain representative curves were determined as true stress = nominal stress(1 + nominal strain) and true strain = ln(1 + nominal strain).[34]

A TA Instruments Q200 differential scanning calorimeter (DSC) was used to analyze the thermal transitions in the PU and the PU−MTM nanocomposites. A small amount (5−10 mg) of the sample was encapsulated in an aluminum pan and heated from −90 to +300 °C at a temperature ramp-up rate of 10 °C/ min and heat change per unit weight was recorded as a function of sample temperature. The enthalpy was obtained by integration of the area under the thermal peaks.

A TA Instruments RSA3 dynamic mechanical analyzer (DMA) was used to measure the storage modulus (E') and tan δ of the PU−MTM nanocomposites. Samples (15 mm by 4 mm) were tested in a uniaxial tension mode with LN_2 gas cooling accessory in the temperature range −100 to +150 °C at a temperature ramp-up rate of 3 °C/min. A constant strain amplitude of 0.25% at a frequency of 1 Hz was applied

Table 1. PU−MTM Nanocomposite Nomenclature

sample name	MTM loading (wt %)	MTM loading (vol %)
PU−MTM7	13	7
PU−MTM10	18	10
PU−MTM12	21	12
PU−MTM16	27	16
PU−MTM26	41	26

throughout the test with an initial static force of 0.01 N. At least 3 samples were tested in order to produce each representative curve.

Results and Discussion

LBL manufacturing allows the preparation of multilayered structures with unprecedented control over the structure at the nanoscale. The organization of LBL nanocomposites has been shown to have striking analogies with the structure of one of the toughest natural mineral-based materials, nacre.[26,32] Recently, we have used the LBL technique to prepare a polyvinyl alcohol (PVA)-MTM nanocomposite with 50 vol % MTM clay nanoparticles that demonstrated a record high average ultimate tensile strength of 400 MPa and an average stiffness of 106 GPa at room temperature (∼23 °C) and humidity of ∼30%.[26] The nanocomposite, however, was brittle with an average ultimate strain-to-failure of 0.003. In a separate work by our group, the effect of humidity on the mechanical properties of LBL nanocomposites was studied.[35] We also showed that the film thickness in LBL manufacturing grows linearly with the number of bilayers and verified the layered structure of LBL nanocomposites using ellipsometry studies.[26,32]

In the present investigation, a series of 300-bilayer PU−MTM nanocomposites with a wide range of volume fractions of MTM nanoparticles was prepared by varying the concentration of PU in solution to vary the thickness of the PU layer deposited in LBL manufacturing (Figure 1A and Table 1). The volume fraction of MTM nanoparticles was inversely related to the thickness of the
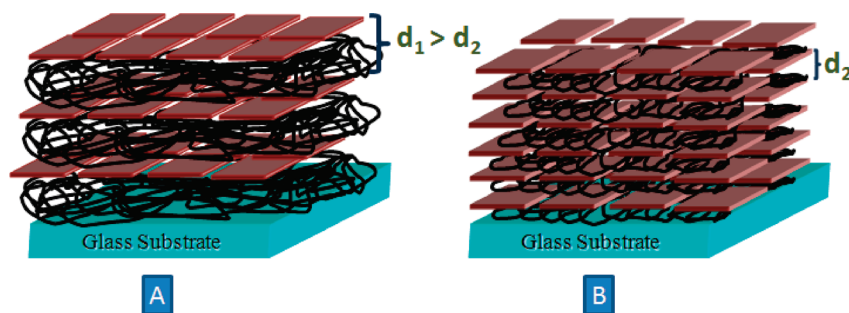
Figure 2. Ideal schematic of nanocomposite structure with (A) lower volume fraction and (B) higher volume fraction of MTM nanoparticles.

PU layer in the nanocomposite. The nanocomposite with a smaller PU layer thickness had a higher volume fraction of MTM nanoparticles than the one having a larger PU layer thickness (Figure 2). The entire series of nanocomposites, however, had a constant MTM dispersion in each nanolayer and constant clay nanolayer thickness. This structural variation facilitated the study of the effect of MTM nanoparticle separation on the mechanics of the PU—MTM nanocomposites.

For a successful LBL deposition, the MTM nanoparticles must create a densely packed layer on the surface of the underlying polymer, which is analogous to Langmuir adsorption.[36] Decreasing the concentration of MTM solution while keeping the immersion time constant would lead to incomplete surface coverage with the MTM nanoparticles and while initially it may allow build up of a few layers, it would eventually lead to termination of the growth process. Increasing the concentration of MTM solution would not affect its loading because after saturation of the adsorbent (MTM) on the surface, mutual repulsion of negatively charged MTM nanoparticles would prevent absorption of further stacks. Additionally, any excess of loosely bound MTM nanoparticles is removed from the surface during the rinsing step.

The TGA thermogram of pure PU revealed poor thermal insulation with almost complete decomposition at ∼500 °C (Figure 1A). Pure MTM clay, on the other hand, did not fully decompose even at a temperature as high as 850 °C and showed a ∼5% decrease in weight. The enhancement of thermal stability, i.e., increased decomposition onset temperature of the nanocomposites with increased volume fractions of MTM nanoparticles, provided evidence of thermo-mechanical interactions between PU and MTM nanoparticles (Figure 1A).

SEM images of the cross sections of 300-bilayer PU—MTM nanocomposites revealed uniform thicknesses (Figure 1B). The thickness decreased with an increase in loading of MTM nanoparticles and was consistent with the thickness of the deposited PU layer (Figure 1C and Table 2).

For LBL manufacturing, the polymer should be water-soluble and preferably charged. The present PU satisfied these requirements (Figure 3A). The presence of a tertiary ammonium group in the short side chain and high density of hydrophilic groups along the backbone impart high solubility in water. The present PU is a block copolymer with alternating soft and hard segments. While the hard segments provided stiffness and strength, large soft segments imparted high ductility to PU. These large proportions of soft segments formed an amorphous domain as examined using the wide-angle X-ray diffraction (WAXD) (Figure 3B). An amorphous peak spanning over a 2θ angle of approximately 10° (from 15° to 25°) was observed in the case of pure PU. The WAXD pattern for the MTM clay showed three distinct peaks in the scan range shown. The lowest angle diffraction peak at a 2θ angle of 7.66° corresponded to a basal (001) spacing of 11.5 Å, suggesting a gallery spacing (i.e., the distance between the silicate layers) of 1.5 Å. The (004) reflection peak was weakly present at a 2θ angle of 19.96° with a calculated basal spacing of 4.45 Å.[37,38]

Other higher-order reflections were very weak reflecting the disorder present in the MTM clay powder.[37,38] In addition to the (001) and (004) reflection peaks, there was a two-dimensional band (02,11) at a 2θ angle of 28.6°, signifying a disordered stacking of the silicate layers.[37,38] The entire series of PU—MTM nanocomposites (Figure 3B) exhibited a small shoulder at a 2θ angle of 6.86° corresponding to a basal (001) spacing of 12.8 Å. This confirmed a constant MTM dispersion within each bilayer in the PU—MTM nanocomposites irrespective of the volume fraction of MTM nanoparticles, as discussed earlier. The disappearance of higher angle (004) and two-dimensional (0,2,11) diffraction peaks confirmed complete exfoliation of silicate in the PU matrix.[37,38] The presence of small-angle shoulder in the PU—MTM nanocomposites indicates that for each MTM nanoparticle deposition step MTM nanoparticles were deposited in multiple layers, suggesting that the multilayered structure of PU—MTM nanocomposites consisted of stratified layers of silicate nanoparticles (each of 1 nm thickness) forming each clay nanolayer (Figure 3 C). The basal spacing of 12.8 Å, or 1.28 nm, was accounted for by the likely presence of water bridges of 0.28 nm between the silicate layers which is reasonably close to the reported values of 1.26 nm for hydrated montmorillonite.[39] The lower bound on the number of silicate layers in each stratified layer may be determined from the minimum average bilayer thickness (cf. Table 2) and volume fraction of MTM nanoparticles associated with it as follows:

$$t_{strat} + t_{pu} = \min(t_b) \quad (2)$$

$$L_{strat} = L_{pu} \quad (3)$$

$$W_{strat} = W_{pu} \quad (4)$$

where t_{strat} is the thickness of the stratified layer (cf. Figure 3 (C)), t_{pu} is the thickness of the PU layer, t_b is the average bilayer thicknesses and $\min(t_b)$ is the smallest value of t_b in Table 2. L_{strat} and L_{pu} are the lengths of the stratified layer and PU layer respectively; and W_{strat} and W_{pu} are the widths of the stratified layer and PU layer respectively. Here, in order to simplify our calculations, we make an assumption that the stratified layer is occupied entirely by MTM nanoparticles.

Using eqs 2, 3, and 4,

$$\frac{t_{strat}}{\min(t_b)} = v_f \quad (5)$$

where v_f is the volume fraction of MTM nanoparticles associated with $\min(t_b)$. t_{strat} is determined as (cf. Figure 3 C):
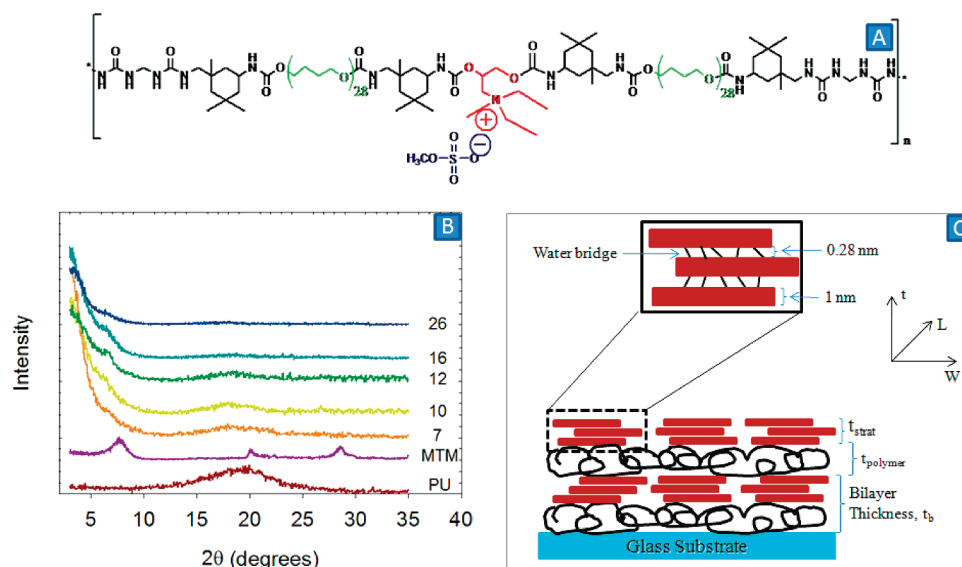
$$t_{strat} = 1(n_s) + 0.28(n_s - 1) \quad (6)$$

Figure 3. (A) Chemical structure of cationic PU copolymer. The cationic functional group of the polymer is highlighted in red, the counterion in blue, the soft segment in green and the hard segment in black. (B) Wide angle X-ray diffraction patterns of PU, MTM clay and PUMTM nanocomposites. Numbers indicate average volume fractions of MTM nanoparticles. (C) Schematic nanostructure of the PU−MTM nanocomposite.

where n_s is the number of silicate layers in each stratified layer. Substituting the value of t_{strat} from eq 5 in 6, a lower bound on n_s is

$$n_s = 2.55 \qquad (7)$$

The upper bound on the number of silicate layers has been determined to be 3 based on a representative volume element description of the nanocomposite structure that differs slightly from that shown in Figure 3(C).[40] It is worth emphasizing here that the deposition of the stratified layers of nanoparticles was the same for all nanocomposites. Therefore, the study of the effect of volume fraction of MTM nanoparticles reduced to a study of the effect of the polymer layer thickness or MTM nanoparticle spacing on the finite deformation response of PU−MTM nanocomposites.

PU−MTM nanocomposites demonstrated an increase in the stiffness, yield strength and ultimate tensile strength when compared with pure PU (Figure 4A, Figure 4B, Table 3 and Table 4). With only 7 vol % of MTM nanoparticles, there was a 10.5-fold increase in the yield strength and an 18-fold increase in the stiffness of the PU−MTM nanocomposite compared to pure PU. The ultimate (nominal) tensile strength increased by a factor of 3.1. The stiffness and yield strength continued to increase with an increase in the volume fraction of MTM nanoparticles. With 12 vol % MTM nanoparticles, the yield strength and stiffness increased 14 and 40 times respectively over pure PU. This enhancement in mechanical properties, viz., stiffness, yield strength and ultimate strength is attributed to the strong MTM nanoparticles alignment parallel to the direction of applied load that allowed a substantial fraction of the load to be transferred to the stiffer, stronger MTM nanoparticles. The ultimate strain-to-failure, however, decreased with increased volume fraction of MTM nanoparticles.

PU−MTM nanocomposites with less than 16 vol % MTM nanoparticles failed in tension with a pronounced yielding of the polymer phase. At 16 vol %, some of the specimens fractured with no yielding while a few specimens failed after yielding (cf. Figure 4C). This is also evident from a large standard deviation on the strain-to-failure value for only this nanocomposite in Table 4. The large variation in strain-to-failure indicates a transition at this volume fraction from ductile to brittle behavior.

Table 2. Thickness of 300-Bilayer PU−MTM Nanocomposites and Average Bilayer Thickness as a Function of Average Volume Fraction of MTM Nanoparticles

sample name	film thickness (μm)	average bilayer thickness, t_b (nm)
PU−MTM7	16.1 ± 1.2	53
PU−MTM10	8.7 ± 0.7	31
PU−MTM12	6.8 ± 0.7	24
PU−MTM16	5.1 ± 0.3	17
PU−MTM26	3.2 ± 0.1	11

Further increase in the volume fraction of MTM nanoparticles resulted in a brittle nanocomposite. The 26 vol % MTM nanocomposite had a strain-to-failure of 0.008 and a stiffness increase of more than 2 orders of magnitude over pure PU. Thus, these nanocomposites demonstrated an increasing stiffness (and yield strength) with nanoparticle volume fraction, in contrast to previous various attempts (Figure 5).[11,12,16−19,23,41] The strain energy at failure (area under the true stress−strain curves) increased 3.25-fold with an incorporation of 7 vol % of MTM nanoparticles when compared with PU (Figure 4D). Further increase in the volume fraction of MTM nanoparticles decreased the toughness due to the decrease in the ultimate strain-to-failure. The energy at moderate strains, however, increased with increasing MTM volume fraction until the volume fraction reached the transition point from ductile to brittle. The energy at 0.5 strain, $U_{0.5}$, increased $\sim$ 10 times with 12 vol % MTM nanoparticles when compared with pure PU (Figure 4D).

We believe that simultaneous improvement in stiffness, strength and toughness in these PU−MTM nanocomposites is the result of both a strong interaction between the MTM nanoparticles and the PU and the control of defects such as regions of particle agglomeration and particle occlusions. The presence of MTM nanoparticles in alternate nanolayers modified the bulk PU in close proximity to the nanoparticles to that of a material composed of confined and stiffened PU chains with restricted mobility.[23,42−44] The PU particle size measured by dynamic light scattering suggested that PU chains attained a similar conformation at all MTM loadings.[45] Since the thickness of the PU layer decreased with an increase in MTM loading, the volume of confined PU chains increased with increased volume fractions of MTM nanoparticles or decreased PU layer thicknesses. An increase in the MTM loading or decrease in the
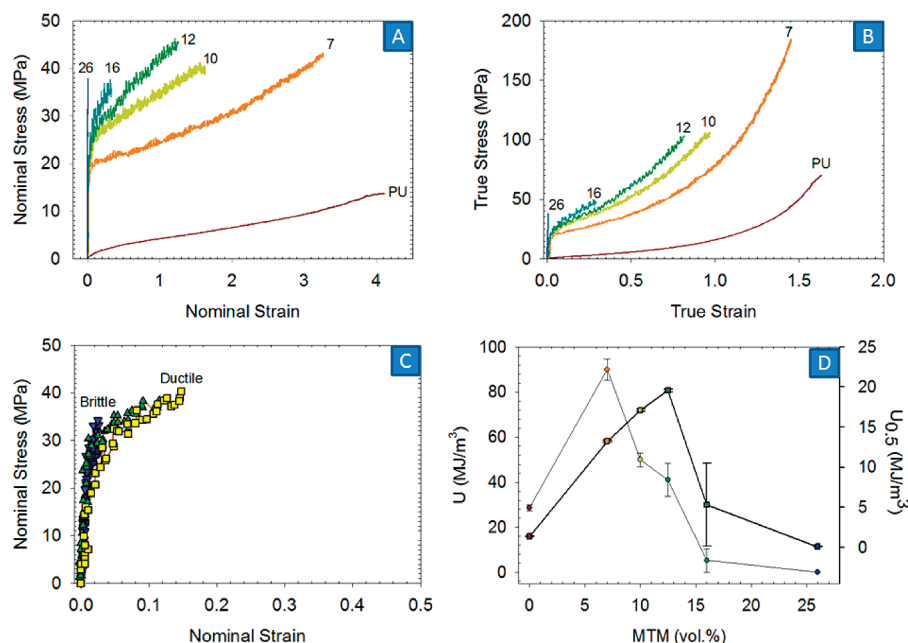
Figure 4. (A) Representative nominal stress−strain constitutive response of PU and PU−MTM nanocomposites. (B) Representative true stress−strain constitutive response of PU and PU−MTM nanocomposites. (C) Representative nominal stress−strain constitutive responses for 16 vol % PUMTM nanocomposite specimens. (D) Strain energy at failure (shown as circular data points) and at 0.5 strain (shown as square data points) for PU and PU−MTM nanocomposites as a function of average volume fraction of MTM nanoparticles. Numbers shown in parts A and B indicate average volume fractions of MTM nanoparticles.

Table 3. Summary of the Mechanical Properties of Pure PU and PU−MTM Nanocomposites

sample name	modulus (GPa)	yield strength (MPa)	modulus ratio (E_{nc}/E_{pu})
PU	0.025 ± 0.005	2.0 ± 0.1	1
PU−MTM7	0.45 ± 0.05	21.1 ± 0.3	18
PU−MTM10	0.74 ± 0.10	25.2 ± 0.4	30
PU−MTM12	1.0 ± 0.2	27.3 ± 0.4	40
PU−MTM16	1.65 ± 0.15	28.5 ± 0.7	66
PU−MTM26	3.6 ± 0.2		144

Table 4. Summary of the Mechanical Properties of Pure PU and PU−MTM Nanocomposites

sample name	ultimate tensile strength (MPa)	ultimate strain
PU	13.2 ± 0.9	4.10 ± 0.10
PU−MTM7	41.2 ± 3.8	3.16 ± 0.10
PU−MTM10	39.5 ± 3.0	1.56 ± 0.08
PU−MTM12	41.0 ± 2.7	1.11 ± 0.09
PU−MTM16	37.4 ± 2.9	0.15 ± 0.14
PU−MTM26	34.2 ± 9.3	0.008 ± 0.003

polymer layer thickness gradually resulted in a transition of bulk PU into confined PU chains, thus resulting in brittle nanocomposites with enhanced stiffness and reduced ultimate strain-to-failure. This transition occurred at 16 vol % MTM nanoparticles corresponding to a polymer layer thickness or MTM nanoparticle separation of ~13 nm (with 3 silicate sheets in each clay nanolayer). Below this separation, brittle behavior dominated the nanocomposite response. At low levels of MTM nanoparticle loadings, the bulk polymer regions were sufficiently mobile and flexible to plastically deform and provide ductility to the nanocomposite response.

The formation of confined polymer chains and their reduced mobility in close proximity to nanoparticles has been addressed previously.[23,42−44,46] For example, Efremov et al. observed the emergence of a pronounced glass transition for polystyrene, poly(2-vinyl pyridine) and poly(methyl mathacrylate) up to thicknesses of 3 nm in close proximity to a platinum surface.[46] However, the present investigation allowed the polymer layer thickness to be the only adjustable parameter in the series of

PU−MTM nanocomposites. This study of the effect of polymer layer thickness on the finite deformation response can further explain the premature failure of nanocomposites containing nonuniform dispersions of nanoparticles as being the result of defects leading to crack formation within regions of poor particle separation, initiating early failure.[12,13,15,16,19]

The effect of polymer layer thickness on the properties of PU−MTM nanocomposites was determined conducting differential scanning calorimetry (DSC) measurements on pure PU and the PU−MTM nanocomposites (Figure 6A). PU exhibited an endotherm at approximately 90 °C indicating a transition to increased thermal motion of PU chains. These thermal transitions were suppressed in the case of PU−MTM nanocomposites (Figure 6, parts A and B). The amount of suppression was found to increase with loading of MTM nanoparticles or decreased polymer layer thickness.

The reinforcing effect of MTM nanoparticles was prominent at the entire observed range of temperatures (Figure 6C). The storage modulus was enhanced at all temperatures and showed an increased stability with an increase in the volume fraction of MTM nanoparticles. The tan δ for pure PU curve showed a peak at about −76 °C, which is attributed to its glass transition temperature (Figure 6D). For the PU−MTM nanocomposites, tan δ was shifted to a slightly higher temperature. This shift of the peak was due to the hindered cooperative motion of the PU chains. The peak value of tan δ was also found to decrease with an increased volume fraction of MTM nanoparticles. This was due to the interfacial interactions between the PU and MTM nanoparticles also observed in the TGA and DSC results.
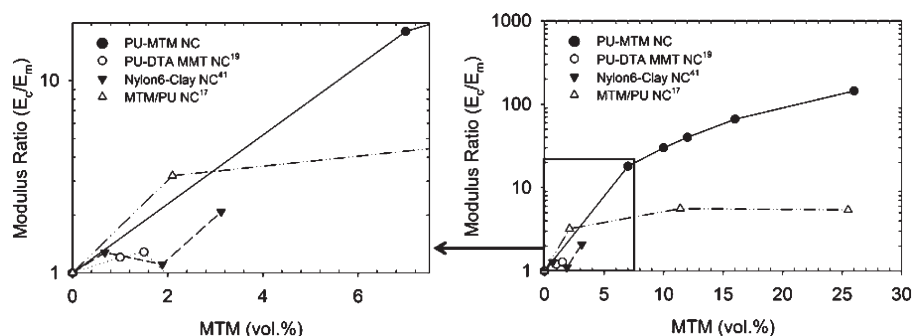
Figure 5. Comparison of enhancement in modulus of PU−MTM nanocomposites with other clay nanocomposites.[17,19,41]
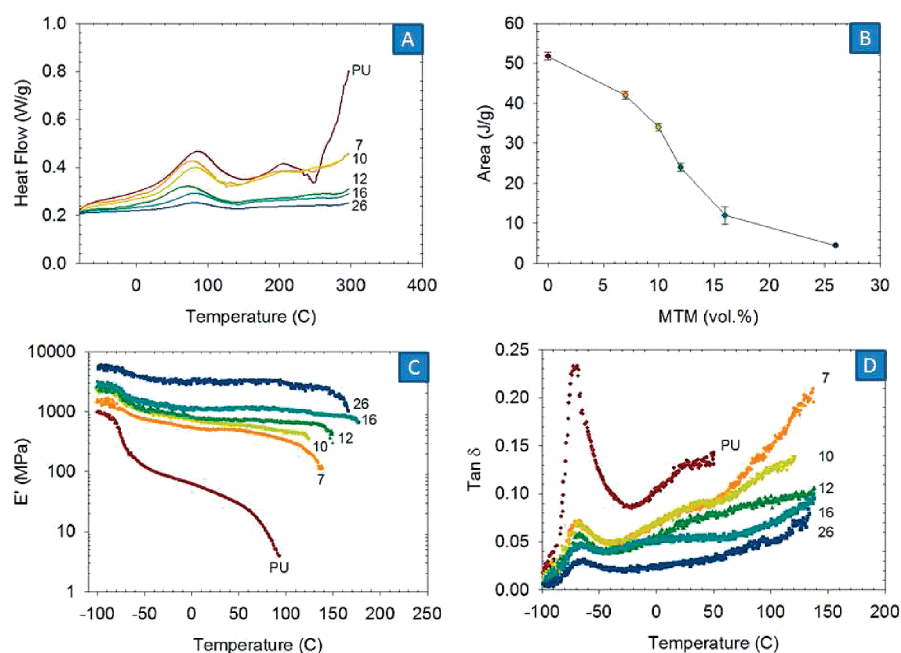

Figure 6. (A) DSC traces of pure PU and PU−MTM nanocomposites. (B) Area under the transition peak for Pure PU and PU−MTM nanocomposites normalized by the amount of PU present. (C) Storage modulus as a function of sample temperature for pure PU and PU−MTM nanocomposites. (D) tan δ as a function of sample temperature for pure PU and PU−MTM nanocomposites. Numbers in parts A, C, and D indicate average volume fractions of MTM nanoparticles.

Conclusions and Future Work. In summary, the role of MTM nanoparticle layer separation in controlling the finite deformation constitutive response of layered polymer− clay nanocomposites has been demonstrated. A series of PU−MTM nanocomposites, with alternating PU and MTM nanolayers, was prepared using the LBL manufacturing technique. LBL allowed us to vary the MTM nanoparticle volume fraction by systematically varying the MTM nano- particle separation while retaining the structural organiza- tion at all volume fractions. The PU−MTM nanocomposites demonstrated enhanced mechanical properties at all volume fractions of MTM nanoparticles, e.g. the yield strength and stiffness increased 14 and 40 times respectively over pure PU with 12 vol % of MTM nanoparticles. The PU−MTM nanocomposite with 26 vol % MTM nanoparticles demon- strated a stiffness increase of more than 2 orders of magnitude.

A transition from ductile to brittle behavior in deforma- tion response was observed at 16 vol % of MTM nanopar- ticles. We demonstrated the existence of a critical MTM nanoparticle separation below which brittle behavior domi- nated the nanocomposite response. Further reduction in MTM nanoparticle separation led to an increased restricted motion of PU chains, resulting in brittle fracture of PU− MTM nanocomposites.

The current investigation addresses the issues facing the design of polymer−clay nanocomposites. The constant dis- persion of MTM nanoparticles over a wide range of volume fractions and the role of the polymer layer thickness in controlling the finite deformation response of nanocompo- sites enabled design optimization in terms of tailoring stiff- ness, strength, and toughness of these nanocomposites. We have also illustrated the current limit of the LBL technology to manufacture PU−MTM nanocomposites with simulta- neously improved stiffness, strength and toughness. Future work will focus on exploring ways to further increase MTM loading while simultaneously maintaining their toughness. Future work will also focus on the development of a con- stitutive model for the finite deformation response of these nanocomposites that is able to predict the change in finite deformation response and the observed ductile to brittle transition.

References and Notes

(1) Sherman, L. M. *Plastics Technol.* **1999**, *45*, 52–57.
(2) Usuki, A.; Kojima, Y.; Kawasumi, M.; Okada, A.; Fukushima, Y.; Karauchi, T.; Kamigaito, O. *J. Mater. Res.* **1993**, *8*, 1179–1184.
(3) Usuki, A.; Kojima, Y.; Kawasumi, M.; Okada, A.; Fukushima, Y.; Karauchi, T.; Kamigaito, O. *J. Mater. Res.* **1993**, *8*, 1185–1189.
(4) Giannelis, E. *Adv. Mater.* **1996**, *1*, 29–35.
(5) Alexandre, M.; Dubois, P. *Mater. Sci. Chem. Soc.* **2000**, *28*, 1–63.
(6) Lan, T.; Pinnavaia, T. *Chem. Mater.* **1994**, *6*, 2216–2219.
(7) Giannelis, E. P.; Messersmith, P. *Chem. Mater.* **1994**, *6*, 1719–1725.
(8) Yano, K.; Usuki, A.; Okada, A.; Karuachi, T.; Kamigato, O. *J. Polym. Sci.: Part A: Polm. Chem.* **1993**, *31*, 2493–2498.
(9) Vaia, R.; Jandt, K.; Cramer, E.; Giannelis, E. *Macromolecules* **1995**, *28*, 8080–8085.
(10) Pinnavaia, T.; Wang, Z. *J. Am. Chem. Soc.* **1998**, *10*, 1820–1826.
(11) Chen, T.; Tien, Y.; Wei, K. *Polymer* **2000**, *41*, 1345–1353.
(12) Zerda, A.; Lesser, A. *J. Polym. Sci., Part B: Polym Phys.* **2001**, *39*, 1137–1146.
(13) Hwang, J.; Liu, H. *Macromolecules* **2002**, *35*, 7314–7319.
(14) Manevitch, O.; Rutledge, G. *J. Phys. Chem. B.* **2004**, *108*, 1428–1435.
(15) Shepherd, P.; Golemba, F. J.; Maine, F. *Adv. Chem. Ser.* **2003**, *134*–141.
(16) Ray, S.; Okamoto, M. *Prog. Polym. Sci.* **2003**, *28*, 1539–1641.
(17) Tortora, M.; Gorrasi, G.; Vittoria, V.; Galli, G.; Ritrovati, S.; Chiellini, E. *Polymer* **2002**, *43*, 6147–6157.
(18) Lagaly, G. *Appl. Clay Sci.* **1999**, *15*, 1–9.
(19) Chang, J.; An, Y. *J. Polym. Sci.* **2002**, *40*, 670–677.
(20) Kojima, Y.; Usuki, A.; Kwasumi, M.; Okada, A.; Karauchi, T.; Kamigaito, O. *J. Polym. Sci., Part A: Polym. Chem.* **1993**, *31*, 983–986.
(21) Okada, A.; Usuki, A. *Mater. Sci. Eng.: C* **1995**, *3*, 109–115.
(22) Fukushima, Y.; Inagaki, S. *J. Incl. Phenom. Soc.* **1987**, *5*, 473–482.
(23) Rao, Y.; Pochan, J. *Macromolecules* **2007**, *40*, 290–296.
(24) Pattanayak, A.; Jana, S. *Polymer* **2005**, *46*, 3394–3406.
(25) Lee, H.; Lin, L. *Macromolecules* **2006**, *39*, 6133–6141.
(26) Podsiadlo, P.; Kaushik, A.; Arruda, E.; Waas, A.; Shim, B.; Xu, J.; Nandivada, H.; Pumplin, B.; Lahann, J.; Ramamoorthy, A.; Kotov, N. *Science* **2007**, *318*, 80–83.
(27) Decher, G. *Science* **1997**, *277*, 1232–1237.
(28) Kotov, N. *Mater. Res. Bull.* **2001**, *26*, 992–997.
(29) Ke, Y.; Stroeve, P. *Polymer-layered Silicate and Silica Nanocomposites*; Chemic Industry: Beijing, 2005.
(30) Lvov, Y.; Haas, H.; Decher, G.; Mohwald, H.; Kalachev, A. *J. Phys. Chem.* **1993**, *97*, 12835–12841.
(31) Ferreira, M.; Cheung, J.; Rubner, M. *Thin Solid Films* **1994**, *244*, 806–809.
(32) Tang, Z.; Kotov, N.; Maganov, S.; Oztruk, B. *Nat. Mater.* **2003**, *2*, 413–418.
(33) Larkin, L.; Calve, S.; Kostrominova, T.; Arruda, E. *Tissue Eng.* **2006**, *12*, 3149–3158.
(34) Malvern, L. *Engineering Mechanics: Statics* Prentice−Hall: Englewood Cliffs, NJ, 1976.
(35) Podsiadlo, P.; Liu, Z.; Paterson, D.; Messersmith, P. B.; Kotov, N. A. *Adv. Mater.* **2007**, *19*, 949–955.
(36) McCullough, D.; Regen, S. *Chem. Commun.* **2004**, 2787–2791.
(37) Wang, A.; D'Souza, N.; Golden, T. *Appl. Clay Sci* **2008**, *42*, 310–317.
(38) Moore, D.; Jr., R. C. *X-ray diffraction and the identification and analysis of clay minerals* Oxford University Press: New York, 1997.
(39) Xu, W.; Johnson, C.; Parker, P.; Agnew, S. *Clay Clay Miner.* **2000**, *481*, 120–131.
(40) Li, Y.; Kaushik, A.; Waas, A.; Podsiadlo, P.; Kotov, N.; Arruda, E. *Manuscript in preparation*, **2009**.
(41) Fornes, T.; Paul, D. *Polymer* **2003**, *44*, 4993–5013.
(42) Vaia, R.; Sauer, B.; Oliver, K.; Giannelis, E. *J. Polym. Sci.: Part B: Polym. Phys.* **1997**, *35*, 59–67.
(43) Ramanathan, T.; Liu, H.; Brinson, L. C. *J. Polym. Sci., Part B: Polym. Phys.* **2005**, *43*, 2269–2279.
(44) Fisher, F.; Eitan, A.; Andrews, R.; Schadler, L.; Brinson, L. *Adv. Compos. Lett.* **2004**, *13*, 105–111.
(45) Kim, H.; Choi, K.; Noh, S. *Manuscript in preparation*, **2009**.
(46) Efremov, M.; Olson, E.; Zhand, M.; Allen, L. *Thermochim. Acta* **2003**, *403*, 37–41.